ACS OMEGA

Article

Cite This: ACS Omega 2019, 4, 8441−8450

http://pubs.acs.org/journal/acsodf

Great Variety of Man-Made Porous Diamond Structures: Pulsed Microwave Cold Plasma System with a Linear Antenna Arrangement

Marián Varga,*[,†] Štepán Potocký,[†] Mária Domonkos,[†,§] Tibor Ižák,[†] Oleg Babčenko,[†,‡] and Alexander Kromka[†,§]

[†]Institute of Physics, Czech Academy of Sciences, Cukrovarnická 10, 162 00 Prague 6, Czech Republic

[‡]Department of Physics, Faculty of Electrical Engineering, Czech Technical University in Prague, Technická 2, 166 27 Prague 6, Czech Republic

[§]Department of Physics, Faculty of Civil Engineering, Czech Technical University in Prague, Thákurova 7, 166 29 Prague 6, Czech Republic

ABSTRACT: Synthetic diamond films are routinely grown using chemical vapor deposition (CVD) techniques. Due to their extraordinary combination of intrinsic properties, they are used as the functional layers in various bio-optoelectronic devices. It is a challenge to grow the dimensional layers or porous structures that are required. This study reviews the fabrication of various porous diamond-based structures using linear antenna microwave plasma (LAMWP) chemical vapor deposition (CVD), a low-cost technology for growing diamond films over a large area (>1 m^2) at low pressure (<100 Pa) and at low temperature (even at 350 °C). From a technological point of view, two different approaches, i.e., templated diamond growth using three different prestructured (macro-, micro-, and nanosized) porous substrates and direct bottom-up growth of ultra-nanoporous diamond (block-stone and dendritelike) films, are successfully employed to form diamond-based structures with controlled porosity and an enhanced surface area. As a bottom-up strategy, the LAMWP CVD system allows diamond growth at as high as 80% CO_2 in the $CH_4/CO_2/H_2$ gas mixture. In summary, the low-pressure and cold plasma conditions in the LAMWP system facilitate the growth on three-dimensionally prestructured substrates of various materials that naturally form porous self-standing diamond structures.

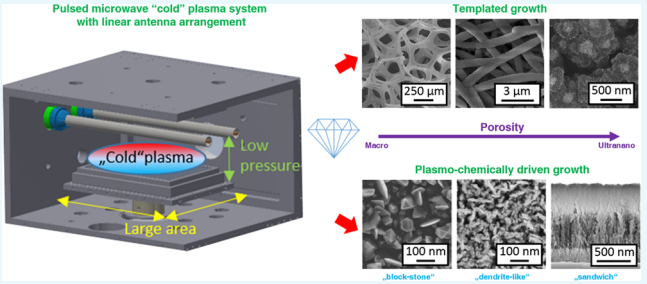

1. INTRODUCTION

Because of their superior properties, synthetic monocrystalline diamonds and polycrystalline diamond thin films have for decades been the focus of interest of various research teams.[1−3] At the same time, diamond is used in numerous industrial fields. As a consequence, various diamond structuring strategies have been developed to fit specific requirements,[4−6] e.g., large surface areas, geometrically ordered microstripes or meshes,[7] nano-objects or nanostructures (wires, rods, and whiskers),[8,9] porous films and membranes,[10,11] etc.

Recently, nanoscaled fibrous materials have been attracting attention due to their specific characteristics, such as high bending performance, flexibility in surface functionalities, a high surface-area-to-volume ratio, and controllable pore size.[12] These advantages make them interesting candidates for a wide variety of applications, e.g., filtration, separation, catalysis, storage and transportation, adsorption, tissue engineering, drug delivery systems, sensors, etc.[8,9,13−15] For example, tailorable pore size is a key requirement in filtration and/or separation.[16,17]

However, fabricating these nanostructures from diamond remains a technological challenge, due to the great hardness of diamond and its chemical inertness or due to undesired diamond graphitization. Ongoing studies have therefore focused on fabricating nanostructures, explaining specific growth phenomena, and developing appropriate technological procedures.

There are two main approaches to diamond film structuring: (i) postgrowth processing (top-down) and (ii) pregrowth (bottom-up) processing. These two approaches differ in the number of technological steps and also in the dimensionality and the geometrical aspect ratios that can be achieved in the structures that are fabricated. Top-down processing involves technological steps, such as depositing a masking material (Al, Ni, Au, Cu, and Pt) followed by plasma etching (generally oxygen with Ar, CF_4, or CHF_3)[5,14] or by thermocatalytically induced etching (graphitization or burning).[11,18] The first study on top-down fabrication of porouslike diamond films was reported by Kriele et al.[16] They fabricated freestanding diamond films consisting of nanopores localized between diamond grains. The porouslike structure was achieved by etching nondiamond carbon forms (mainly localized along grain boundaries) by annealing in air at elevated temperatures (530−560 °C).

Received: February 4, 2019
Accepted: April 19, 2019
Published: May 14, 2019

DOI: 10.1021/acsomega.9b00323
ACS Omega 2019, 4, 8441−8450

Bottom-up processing is either guided by selective area nucleation/deposition or is achieved by direct growth on prestructured substrates, porous membranes, or nanofibers.[4,6,15] Key benefits are minimal technological steps and a larger variety of complex geometries. However, the main limitation is the less precise fabrication of structures, due to (i) the pyramidlike diamond growth of the crystals and (ii) the hard-to-control vertical and lateral diamond growth. Using the bottom-up approach, porosity of the diamond films is achieved by either (i) employing geometrically prestructured substrates (i.e., templated growth) or (ii) optimized chemical vapor deposition (CVD) by providing suitable growth conditions (mainly by varying the gas mixture). The variety of supporting substrates includes fully or partially transformable polymers,[19−21] various non-carbon-based templates,[14,17,22,23] carbon-based templates,[24−28] or SiO_x-based templates.[29−31] The important advantage of templated diamond growth is that the porosity is generally guided by the template that is used.[27,30,32] In the course of the development and usage of these supports, various aspects of procedures that can be used and specific applications have already been discussed. For example, diamond nanoparticles in a polymer matrix can be used for fabricating porous diamond structures,[7,19] for enhancing the seeding efficiency in planar diamond deposition and for diamond growth on vertical structures.[20,33,34] In the case of diamond deposition on graphitelike materials, the proper seeding technology and the chemical stability of these materials has a direct effect on the final geometry of the structure that is formed.[26,27] In addition, the pore size of the templates has a strong influence on the penetration of the growth species in depth (i.e., in the *Z*-direction) during chemical vapor deposition (CVD). Pore size therefore has an impact on the final thickness of a porous diamond-based structure.[10,30,35]

This can be overcome by using layer-by-layer deposition,[29,31,32] but it is a time-consuming and expensive procedure. For direct growth of thick porous diamond layers, steady kinetic reactions during CVD are required to achieve porous growth rather than micro- or nanocrystalline growth.[36,37] A reliable technique for templated and direct fabrication of porous diamond structures is highly sought after.

In this paper, we introduce the linear antenna microwave plasma (LAMWP) CVD system as a promising "4L" (low-pressure, low-temperature, low-cost, and large-area) technology for fabricating a great variety of porous diamond-based structures. We present and summarize five complementary bottom-up technological processes suitable for fabricating diamond-based structures with different porosities. Two approaches are involved: (1) templated diamond growth on porous substrates, including (i) carbon foam (C-foam) with macrosized porosity, (ii) a nonwoven nanofibrous SiO_x mat with microsized porosity, (iii) buckypaper (BP) composed of single-wall carbon nanotubes (SWCNT) with nanosized porosity, and (2) direct plasmochemically driven growth of (i) block-stone-like and (ii) dendritelike diamond films with ultra-nanosized porosity. All of these approaches allow the fabrication of self-standing three-dimensional (3D) diamond-based porous structures with the use of just one CVD system.

2. EXPERIMENTAL PART

2.1. Materials and Preparation. The LAMWP CVD system consists of a water-cooled chamber with two linear Cu conductors (≈60 cm in length) located inside quartz tubes. A distributed gas inlet enables a homogeneous precursor input over the complete length of the antennas. Microwave power is delivered from both sides by two microwave generators (2.45 GHz, Muegge) working at pulse-frequency up to 500 Hz and at maximum power up to 4.4 kW in a pulse, using a specially designed splitter-adapter (Muegge GmbH). The plasma is generated in an asymmetric way between the two electrodes and ground.[38] This configuration provides homogeneous plasma distribution at low working pressure (units of Pa) over the water-cooled graphite substrate holder 30 × 20 cm^2 in area.[39] The design principle and corresponding reaction mechanism (simplified for H_2 plasma) of such a deposition system can be found in ref 40. The distance between the substrate holder and the antennas (*Z*-axis distance) can be adjusted in the range of several centimeters and was fixed at 7 cm in this work. At this distance, the effective electron temperature T_{eff} is about 1.5 eV,[41] i.e., the LAMWP system is characterized by a cold MW plasma process at the surface of the substrate. This setup allows diamond growth at low temperature (250 °C).[42] However, if needed, the substrate temperature can be controlled independently of the CVD process by a resistively heated substrate holder up to 800 °C.[43] In this study, we performed diamond deposition at temperatures in the range between 350 and 650 °C in a $CH_4/CO_2/H_2$ gas mixture. The porous diamond structures were fabricated either by novel CVD growth on a planar substrate or by low-pressure CVD growth on macro-, micro-, and nanoporous templates.

A commercially available rigid and highly porous (80 pores per in.) C-foam was used as a macrosized porous template.[44] The C-foam (15 × 10 × 3 mm^3) was first oxidized by RF oxygen plasma to make its surface hydrophilic. On the basis of the previously optimized nucleation and growth procedures,[27] the C-foam was seeded for 10 min in a poly(vinyl alcohol)/nanodiamond (50:50 ratio) mixture, using an ultrasonic bath.

The microsized porous template was a silica (SiO_x) nonwoven three-dimensional nanofibrous mat produced by needleless electrospinning (NanoSpider, Elmarco Ltd.). The mat consisted of randomly oriented submicron fibers (ø ≈ 100 nm) weighing 20 g m^{-2}, and the total thickness of the mat was about 60−70 μm. The large SiO_x mat was cut into smaller pieces (3 × 4 cm^2) and was treated in RF oxygen plasma to achieve a hydrophilic character. The prepared mats were then seeded by soaking in a dispersion of deionized water and ultradispersed detonation diamond (UDD, ø ≈ 5−10 nm, New Metals and Chemicals Corp. Ltd.).

Finally, a buckypaper (BP) composed of single-wall carbon nanotubes (SWCNTs) was used as the nanosized porous template. The fabrication procedure is described in ref 45. In brief, the SWCNTs were first dispersed in an *n*-methyl pyrrolidone solution and were then filtered through the nylon membrane by vacuum filtration to fabricate a self-standing dense SWCNT BP. The BP substrate was approximately 8 μm in thickness. Before the diamond CVD, the BPs were immersed in deionized water with UDD for 30 min.

The ultra-nanoporous (block-stone and dendritelike) diamond films were fabricated on mirror-polished Si(100) substrates 1 × 1 cm^2 in size, which were ultrasonically seeded in a suspension of deionized water and UDD. Similarly, silicon substrates coated with ultrananno- (UNCD) and microcrystalline diamond (MCD) layers were also used, but no ultrasonic treatment was performed on them.

The substrates with various porosities and diamond CVD growth conditions are presented in Table 1.

DOI: 10.1021/acsomega.9b00323
ACS Omega 2019, 4, 8441−8450

Table 1. Different Porosities and Applied Diamond Growth Conditions of the Substrates

description	diamond film porosity	deposition time (h)	microwave power (kW)	$CH_4/CO_2/H_2$ gas flow (sccm)	substrate temperature (°C)
SET 1 diamond growth on C-foam	macroporous (substrate template)	60	2 × 2	10:0:100	650
SET 2 diamond growth on SiO_x mat	microporous (substrate template)	60	2 × 2	5:20:150	550
SET 3 diamond growth on SWCNT BP	nanoporous (substrate template)	15	2 × 1.7	5:20:50	450
SET 4 growth of porous (block-stone and dendritelike) diamond films	ultra-nanoporous (self-template)	15	2 × 1.7	5:20:50	450
				5:20:25	650
					550
					450
					350

2.2. Materials Characterization. The surface morphology and the grain size of the fabricated diamond films/structures were analyzed using a field-emission scanning electron microscope (SEM) operating in secondary electron mode (MAIA3, Tescan Ltd.) and in semi-in-lens mode (JSM7500F, JEOL). The diamond character of the deposited films was determined by Raman spectroscopy (InVia, Renishaw) using a He−Cd laser with 325 and/or 442 nm excitation wavelengths.

3. RESULTS AND DISCUSSION

3.1. Templated Diamond Growth. *3.1.1. Macrosized Porosity: Diamond Growth on C-Foam.* The structure with macrosized porosity was produced by templated growth of a diamond film on C-foam. In general, it is not a simple task to grow diamonds on this kind of graphite-based material using high-density MW plasma CVD, due to the presence of atomic hydrogen and oxygen species in the plasma, which degrades and etches this material. One solution is to use a poly(vinyl alcohol) and UDD mixture for the nucleation of C-foams, followed by diamond growth.[27] It should be noted that successful overgrowth of porous C-foams by a continuous diamond film within the whole volume of the substrate (3D growth) was achieved only by the LAMWP CVD. Representative SEM images of the bare and diamond-coated C-foams are shown in Figure 1a,b. The presence of the diamond film is confirmed by Raman spectroscopy (Figure 1c). The Raman spectrum of the bare C-foam consists of two bands known as the D band (defect sp^2 phases), centered at 1356 cm^{-1}, and the G band (graphitic phases) centered at 1585 cm^{-1}. Compared with the bare C-foam, the Raman spectra of the diamond-coated C-foam taken from the top and the bottom side reveal a red-shift of the position of the D band from 1356 to 1332 cm^{-1}. Additionally, the band at 1150 cm^{-1}, which is attributed to *trans*-polyacetylene (*t*-PA) chains at diamond grain boundaries, is also present. The diamond morphology taken at three different depths through the C-foam is shown in Figure 1d. The diamond coating is present throughout the bulk of the macroporous C-foam framework. However, due to the variations in the penetration efficiency of the active species within the *Z*-scale (~3 mm), a visible difference in the thickness of the diamond film is observed, i.e., delayed closing/growing of the diamond film was achieved at the bottom of the substrate. However, this delay can easily be solved by a prolonged deposition time. Similar results (not shown here) were also observed for C-foams with lower porosity (60 pores per in.) and with higher porosity (100 pores per in.).

We will now discuss the homogeneity of the deposited diamond film within the C-foam volume (bulk) achieved in our LAMWP system. Marton et al.[25] also exposed C-foam to

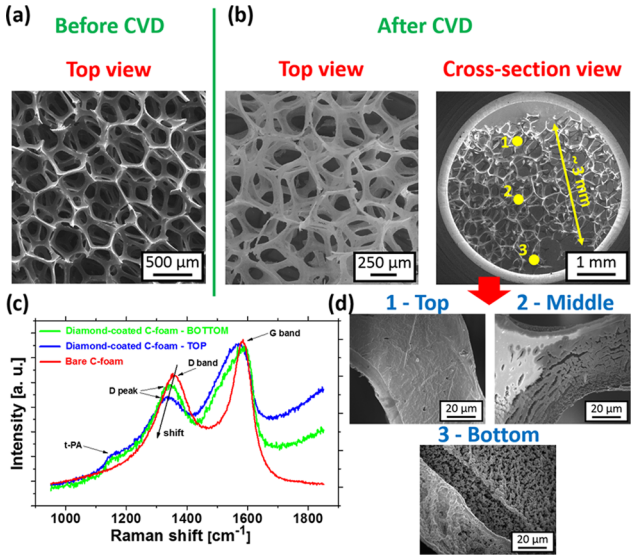

Figure 1. SEM images of the (a) bare and (b) diamond-coated C-foams. (c) Raman spectra of the bare and diamond-coated C-foams (top and bottom side) measured with the 442 nm excitation wavelength. (d) SEM images of the diamond-coated C-foam taken from the top to the bottom of the substrate (i.e., *Z*-depth profiling).

the diamond growth process in a hot filament (HF) CVD system. They observed the formation of various carbon-based materials (diamond, carbon nanowalls, graphite nanosheets, etc.) within the volume of the C-foam, depending on the *Z*-distance from the hot filaments. Marton et al. also reported a strong influence of the porosity of the foam on the deposited structures. The diamond growth rate decreased rapidly or there was even no diamond growing inside the C-foam volume with increased porosity. This was attributed to a lack of atomic hydrogen penetrated into the C-foam. Thanks to the significantly lower working pressure in the LAMWP CVD system than that in the HF CVD system (i.e., 10 vs 3000 Pa), deeper penetration of the growth species into the C-foam volume should be achieved and any formation of nondiamond forms is effectively suppressed. Other types of materials with similar porosity (e.g., silicon carbide or alumina foam, etc.) can be used to minimize any complications related to carbon-based substrates (damage to the substrate and substrate etching).

3.1.2. Microsized Porosity: Diamond Growth on a SiO_x Mat. Self-standing porous diamond membranes were fabricated using templated growth on three-dimensional microporous SiO_x fiber mats. The template (mat thickness, average fiber diameter, pore size, and the relative spacing between the fibers) was primarily defined by the parameters of the electrospinning process. Figure 2a shows a top-view SEM

DOI: 10.1021/acsomega.9b00323
ACS Omega 2019, 4, 8441−8450

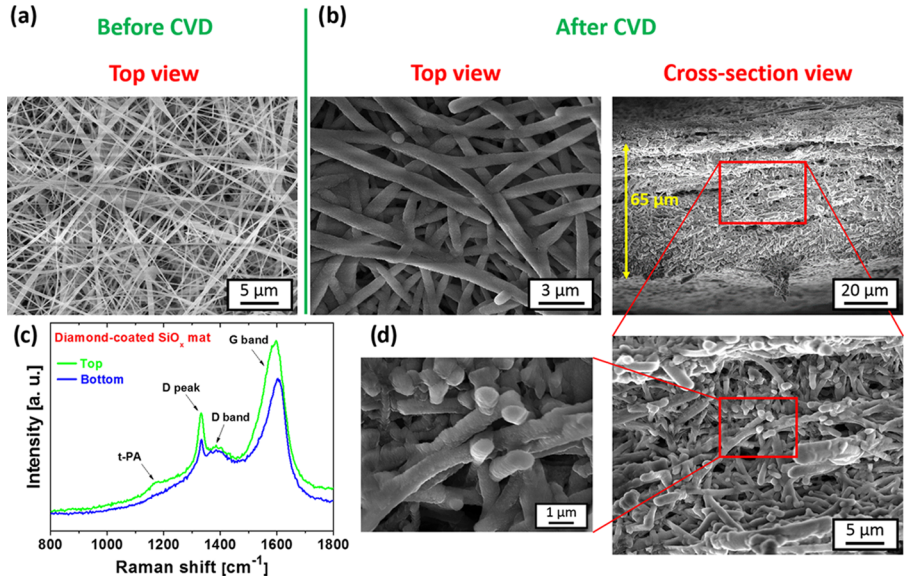

Figure 2. (a) Top-view SEM image of the bare SiO_x fiber mat. (b) Top-view, cross-sectional view, and (d) detailed-view SEM images of the SiO_x fiber mat after diamond deposition. (c) Raman spectra of the top and the bottom of the diamond-coated SiO_x mat measured with the 442 nm excitation wavelength.

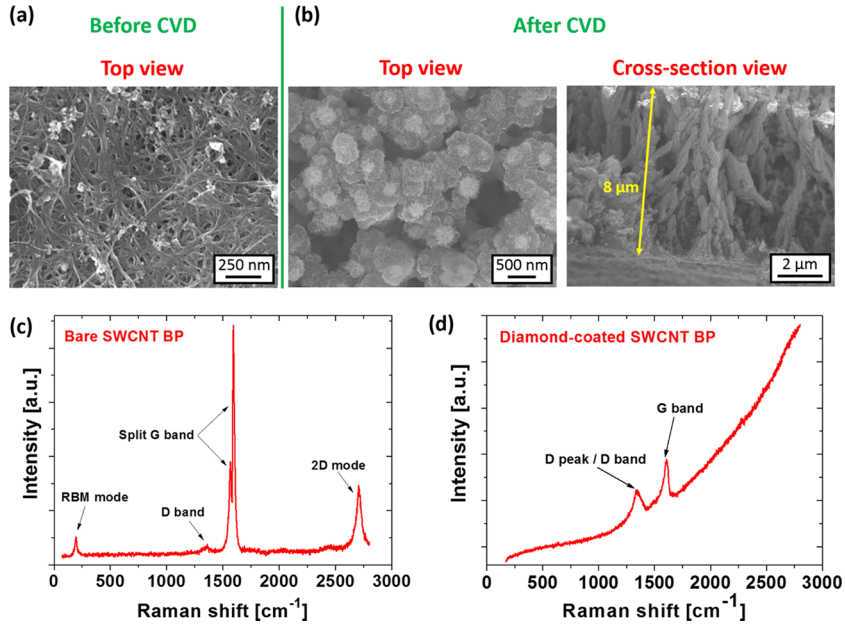

Figure 3. (a) Top-view SEM image of the bare SWCNT BP. (b) Top-view and cross-sectional-view SEM images of the diamond-coated SWCNT BP. The corresponding Raman spectra of the (c) bare and (d) diamond-coated SWCNT BP samples, measured with the 442 nm excitation wavelength.

image of the electrospun fiber mat, which comprises randomly oriented SiO_x fibers with submicron diameter and a smooth surface. Figure 2b shows top and cross-sectional views of the nanofiber mat after the diamond CVD process. Detailed views (see Figure 2d) confirm a hermetic coating of SiO_x fibers with the diamond film.

Some authors have reported that diamond deposition on a fibrous template dominates only on the top surfaces whereas other layers shield the inner part from plasma, resulting in nonuniform diamond growth within the *Z*-depth.[10,31] The reason for this was assigned to hindered diffusion and penetration of reactive species into the bulk of the densely packed fibrous template.[30,32] To improve the homogeneity of the diamond film growth with the template bulk, polymers have been used as the seeding layer[30] or a layer-by-layer deposition process has been used.[31] As has already been demonstrated above, the LAMWP system naturally forces diamond growth also on 3D substrates (i.e., on perpendicular walls of prestructured substrates). Its low-pressure operation mode (10 Pa) prolongs the mean free path of active species and therefore naturally suppresses any limitations in diffusion.[10,30,32]

It should be noted that oxygen plasma pretreatment and subsequent seeding with diamond nanoparticles also ensured homogeneous nucleation throughout the volume of the template by the opposite surface charges of UDD[46] and SiO_x

DOI: 10.1021/acsomega.9b00323
ACS Omega 2019, 4, 8441−8450

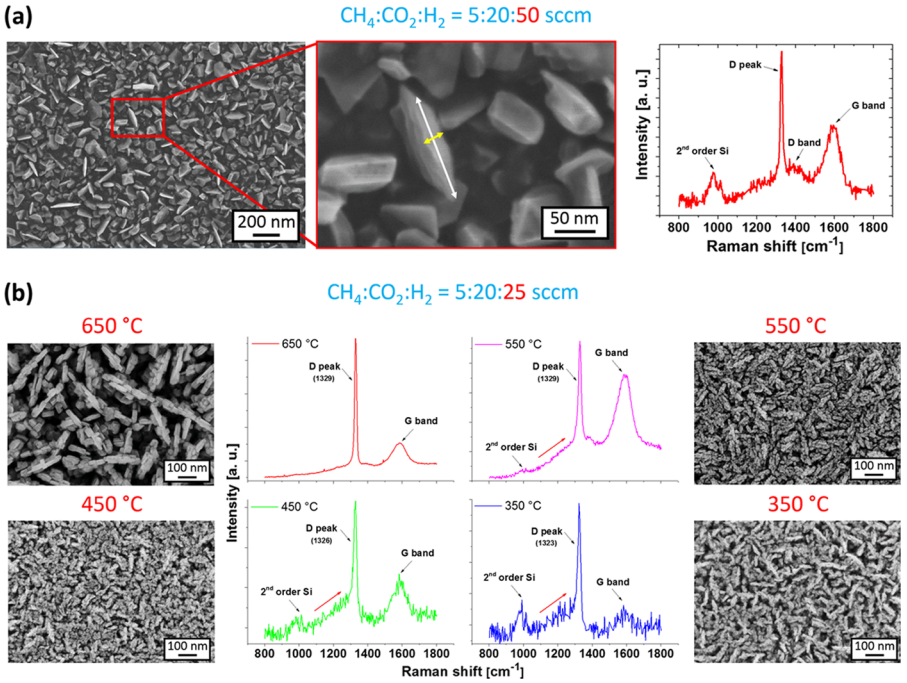

Figure 4. (a) SEM images and the Raman spectrum of a block-stone diamond film deposited at a temperature of 450 °C from a gas mixture of $CH_4/CO_2/H_2$ = 5:20:50 sccm. (b) Top-view SEM images and the corresponding Raman spectra of dendritelike diamond films grown at different deposition temperatures and with a higher CH_4 + CO_2 content in a gas mixture ($CH_4/CO_2/H_2$ = 5:20:25 sccm). The Raman spectra were measured with the 325 nm excitation wavelength.

fibers. No mixing with polymer matrix[30,31] was therefore necessary in our case. The fibers were well-overgrown by the diamond film throughout the 65 μm thickness of the substrate; see Figure 2b. Moreover, the diamond film well copied the initial microstructure of each individual fiber. We were also able to coat the whole membrane efficiently, using two-sided deposition in a single run. In this case, the fiber mats were mounted on a special substrate holder (i.e., the templates "hovered" ∼1 cm above the substrate holder), which enabled simultaneous chemical vapor deposition on both sides, i.e., on the top side and on the bottom side. No major morphological changes were observed for the top and bottom parts of the diamond-coated SiO_x mat, which indicates almost identical films.

These results are also supported by Raman measurements, i.e., the Raman spectra from the top and from the rear side are similar (see Figure 2c). In general, both Raman spectra are dominated by the diamond characteristic peak centered at 1332 cm^{-1} and by two broad bands at 1385 and 1600 cm^{-1}, which are attributed to the D band and the G band, representing the nondiamond carbon bonds (sp^2 phases) in the diamond film.[47] The weak band centered at 1168 cm^{-1} corresponds to *trans*-polyacetylene groups localized mainly at grain boundaries. The LAMWP system also ensured excellent deposition homogeneity over large areas; i.e., 18 samples 3 × 4 cm^2 in size were coated within a single deposition run.

3.1.3. Nanosized Porosity: Diamond Growth on SWCNT Buckypaper. Finally, we report on templated diamond growth on very densely packed SWCNT buckypaper with nanosized porosity. Figure 3a shows the top-view SEM image of the bare buckypaper substrate, which is primarily composed of SWCNT bundles, with only a small amount of impurities (amorphous and carbonaceous residues). The corresponding Raman spectrum (Figure 3c) reveals four characteristic peaks/bands: (i) radial breathing mode at 193 cm^{-1}, (ii) the D band at 1360 cm^{-1}, (iii) the split G band (G^- and G^+ at 1566 and 1593 cm^{-1}, respectively), and (iv) two-dimensional (2D) mode at 2705 cm^{-1}. After the diamond CVD process, the SWCNT bundles were homogeneously coated with a nanocrystalline diamond (NCD) film (Figure 3b) not only on the top of the substrate but also throughout the volume of the porous BP (see the cross-sectional SEM image in Figure 3b). This compact diamond coverage led to significant changes in the Raman spectrum (Figure 3d), which is now dominated by two bands recognized as the D band (a broad band combining the diamond peak 1333 cm^{-1} and the red-shifted defect band 1348 cm^{-1}) and the blue-shifted G band to 1607 cm^{-1}.

In the case of diamond growth on SWCNT BP, both the low working pressure and the gas composition are crucial parameters. The gas composition has to be chosen very properly to avoid the formation of a two-layer compartment heterostructure, due to the rapid diamond growth rate and, at the same time, to avoid the rapid substrate etching by atomic hydrogen. Moreover, the typically used $CH_4/CO_2/H_2$ gas mixture in the LAMWP system results in more complex plasmochemical reactions than in the conventionally used CH_4/H_2 atmosphere. The main role of the added CO_2 gas is to increase the diamond growth rate and to improve the diamond quality.[48] However, the presence of oxygen species together with atomic hydrogen species makes the plasma environment more aggressive, especially for the nondiamond carbon-based substrates.[49] However, unconventional diamond growth can be achieved at an unusually high ratio of CO_2 to H_2 (see Section 3.2).

As a summary of Section 3.1, the pulsed microwave cold plasma system with a linear antenna arrangement is versatile for the production of various porous diamond structures with adjustable morphologies. The low-pressure operation length-

DOI: 10.1021/acsomega.9b00323
ACS Omega 2019, 4, 8441−8450

ens the homogeneity of the diamond growth in the substrate Z-depth and also enhances the penetration of the growth species into the porous templates. However, the pore size is still a substantial parameter because penetration of the growth species is clearly easier (simpler) for large (macro-) pores than for smaller (micro- and nano-) pores. Thanks to the large distance of the microwave plasma from the substrate, the LAMWP system also enables two-sided deposition in a single run and homogeneous diamond growth in the volume of thick or densely packed porous templates. Moreover, the LAMWP system can vary the deposition conditions (temperature and gas composition) in a wide range to tailor the thickness, the morphology, and the crystalline quality of the diamond coating to specific needs. It should be noted that boron-doped diamond films can also be prepared by this system, which widens the applicability of porous diamond structures.

3.2. Ultra-Nanosized Porosity: Plasmochemically Driven Porous Diamond Growth. Porous (block-stone and dendritelike) diamond films were also directly grown on standard seeded polished silicon substrates or on polycrystalline diamond films deposited on silicon in the pulsed microwave cold plasma system with a linear antenna arrangement. Using the same deposition conditions (see Table 1) as those for the overgrowth of the SWNCT BP templates, we observed homogeneous coverage of Si with well-faceted block-stone diamond crystals (Figure 4a). Some crystals exhibit platelike structures, i.e., quasi 2D diamond crystallites around 20 nm in thickness (yellow arrow) and up to 200 nm in lateral dimension (white arrow). The length-to-thickness aspect ratio was approximately 10. Although the surface is homogeneously covered with diamond crystals, these plates are sparsely located (see Figure 4a). The Raman spectrum consists of the diamond characteristic peak centered at 1329 cm^{-1} and two broad bands centered at 1388 and 1588 cm^{-1}, known as the D band and the G band, respectively (Figure 4a). The band at around 981 cm^{-1} is attributed to the second order of silicon.

Similar block-stone diamond crystals have already been prepared at high temperatures (>850 °C) using the ASTeX resonant cavity MW plasma enhanced CVD system.[50−53] However, high-temperature diamond growth is applicable only for limited substrate materials, e.g., silicon. Drijkoningen et al. have recently reported the growth of diamond plates in a linear antenna microwave plasma system at a lower temperature (410 °C), using MW continuous wave power of 2.8 kW, a gas mixture of $CH_4/CO_2/H_2$ (2.5% CH_4 and 6% CO_2 to H_2), and a low working pressure of 23 Pa.[37] The diamond plates were randomly oriented and were up to 130 nm in height after 18 h. For the prolonged deposition time (up to 64 h), the individual plates disappeared and only a continuous layer consisting of microcrystalline diamond grains was observed. The driving force for the anisotropic growth of the plates was assigned to the stacking faults present in the early stages of the diamond growth.[36] Drijkoningen et al. proposed a model in which the formation of diamond plates is related to silicon atoms, i.e., "impurity traces" coming from the quartz tubes. Here, Si atoms were involved as a catalyst that either blocks diamond layer growth or enhances the selective etching of {111} diamond facets (for details, see ref 37). Drijkoningen et al. reported that once the diamond crystals enlarged their size enough, the plate growth collapsed and microcrystalline grains dominated the surface morphology of the sample. On the basis of their model, the growth of thick porous structures (500 nm and larger) therefore seems to be unfavorable at these process parameters. However, this contrasts with our findings.

Note that the gas mixture and the total gas pressure are crucial process parameters that influence the quality and the morphology of the diamond films. In our previous studies, we have demonstrated that the addition of a small amount of CO_2 to the CH_4/H_2 gas mixture substantially improved the diamond growth.[39] Next, taking into account the Bachmann ternary diagram, the diamond growth should be suppressed usually at a high oxygen content (>40% CO_2 in the CH_4/H_2 gas mixture).[54] However, the diamond growth in LAMWP CVD does not strictly follow the Bachmann ternary diagram and the diamond also grows at higher CO_2, i.e., outside the forbidden region.[55]

Another issue is the total gas pressure in the LAMWP system. At process pressure >100 Pa, the diamond growth was dominated by the renucleation mode and the films that formed consisted of nanosized diamond crystals (<50 nm) with a high content of sp^2-bonded carbon on grain boundaries.[41] However, reducing the pressure to 10 Pa (in our case) suppressed the renucleation mode[43] and the crystal size increased in proportion with the deposition time. In this case, the Raman spectrum revealed a sharp diamond peak. In this sense, the combination of high CO_2 content (40% to hydrogen) and low process pressure (10 Pa) allows the formation of a high-quality diamond in a block-stone form (Figure 4a), whereas higher CO_2 content (80%) results in the formation of a dendritelike form (Figure 4b). In general, the low working pressure increases the concentration of atomic hydrogen, thus locating the points on the triangular Bachmann diagram closer to the hydrogen vertex.[56] We assume that the increased CO_2 content, i.e., the increased amount of oxygen-based species (such as CO, CO_2, O_2, or alcohol) supports the role of atomic hydrogen and has a beneficial effect on the diamond growth regime. In addition, the higher CO_2 content led to formation of a higher amount of OH radicals[57] and in combination with a low-pressure regime, it finally switched the diamond growth regime from a block-stone to dendritelike form. In comparison with the block-stone diamond, the growth of the dendritelike diamond can be tailored by the deposition temperature. Although all of the Raman spectra reveal a high-quality diamond film with just a small amount of sp^2 hybridized carbon, some changes can be still observed. The diamond films deposited at higher temperatures (650 and 550 °C) are characterized by three Raman features: (i) the diamond peak centered at around 1329 cm^{-1}, (ii) the D band with a maximum at 1388 cm^{-1}, and (iii) the G band at 1585 cm^{-1}. Lowering the deposition temperature resulted in a red-shift of the diamond peak to a value of 1323 cm^{-1} and a clear increase in the diamond peak shoulder around 1250 cm^{-1}. This feature most likely originates from a disordered sp^3 phase, which is typically found in dynamically synthesized nanodiamonds and may be a part of the sp^3/sp^2 near-surface stress-releasing transient layer.[58]

For the growth of isolated diamond nanowires, (111) nanowires were proposed as the unstable form whereas C(100)(2 × 1) dimer rows parallel to the axis of the nanowire should ideally fulfill the stability requirements.[59] Theoretical calculations later showed that certain morphological criteria must be fulfilled for structurally and thermodynamically stable diamond nanowires or nanorods.[60] This may be the reason why the chemical and kinetic reactions are in thermodynamic equilibrium with the etching process and the growth of the

DOI: 10.1021/acsomega.9b00323
ACS Omega 2019, 4, 8441−8450

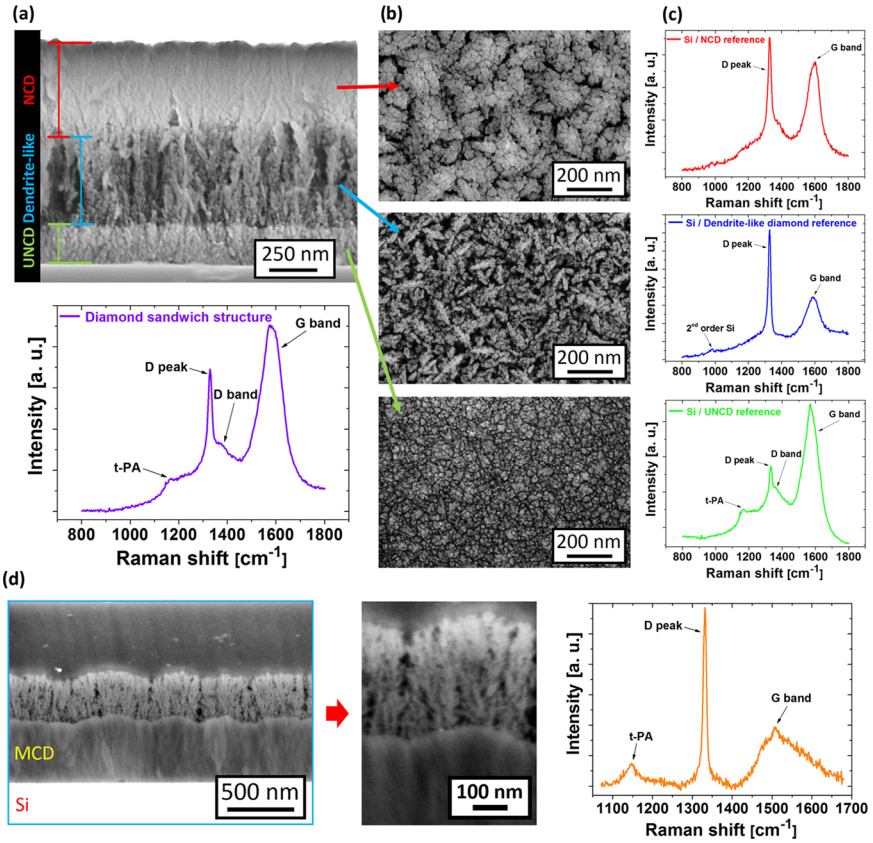

Figure 5. (a) Cross-sectional view of the diamond sandwich structure (UNCD/dendritelike/NCD) and the corresponding Raman spectrum of the final sandwich structure. (b) Top-view SEM images of the diamond structures after an individual deposition step during fabrication of the sandwich structure, and (c) the corresponding Raman spectra of the reference diamond films deposited on silicon substrates measured with the 325 nm excitation wavelength. (d) Cross-sectional SEM images and the Raman spectrum measured with the 442 nm excitation wavelength of the MCD/dendritelike diamond structure.

preferential crystallographic orientation. This type of specific equilibrium could also be required for dendritelike diamond growth, as presented in this work. Dendritelike diamond growth seems to be driven only by plasmochemical processes (and not to be influenced by the substrate material), and it does not collapse into micro- or nanocrystalline diamond growth for prolonged deposition times.

Further evidence for a plasmo-hemical driven process is demonstrated by the dendritelike diamond growth on ultrananno- (UNCD) and microcrystalline (MCD) diamond films. Figure 5a shows a cross-sectional view of a diamond sandwich structure. The diamond sandwich structure starts with the UNCD base layer, which was further used as a substrate for the growth of dendritelike diamond. Finally, the dendritelike porous structure was overgrown with nanocrystalline diamond (NCD). Figure 5b shows top-view SEM images of individually deposited diamond films on planar Si substrates (the reference). The dendritelike diamond growth is not conditioned by the UNCD morphology and reveals the same morphology as in the previous section (Figure 4b). However, the NCD film well copies the top profile of the dendritelike diamond layer.

Figure 5a shows the Raman spectrum of the final sandwich structure. For comparison, Figure 5c shows the corresponding Raman spectra of each diamond type deposited on Si substrates. It is evident that the Raman spectrum of the sandwich structure is primarily influenced by the UNCD layer. However, the diamond peak intensity and the contemporaneous lower G band intensity seem to be related to higher-quality diamond films (dendritelike and NCD films).

Finally, a two-layer compartment of the dendritelike diamond film (deposited at T = 450 °C) on a rough microcrystalline diamond film was also fabricated. It is evident from the cross-sectional SEM images that the dendritelike growth is not disturbed (influenced) by the base MCD layer (Figure 5d). The Raman spectrum is characterized by three typical features: *t*-PA, the diamond peak, and the G band. Unlike in the sandwich structure, the position of the diamond peak (1331 cm^{-1}) is preferentially influenced by the MCD layer (Figure 5d). Finally, it should be noted that dendritelike diamond growth was also observed on nonseeded Si substrates, due to spontaneous nucleation (not shown here).

To summarize Section 3.2, the unconventional diamond growth regime that is outside the Bachmann ternary diagram led to the direct growth of porous block-stone and dendritelike diamond films. Both of these growth modes are affected by the low total gas pressure (10 Pa) and by the composition of the gas, with a high content of CO_2 gas (40% CO_2 to H_2 for porous block-stone and 80% CO_2 to H_2 for dendritelike diamond films). The diamond growth itself is mainly driven by plasmochemical reactions, i.e., it is not conditioned by the substrate material. Moreover, the dendritelike diamond growth does not collapse after reaching a certain diamond film thickness. This is in contrast to the block-stone growth model.[37] This unique bottom-up porous diamond growth, observed only when there is a high CO_2 content in the

DOI: 10.1021/acsomega.9b00323
ACS Omega 2019, 4, 8441−8450

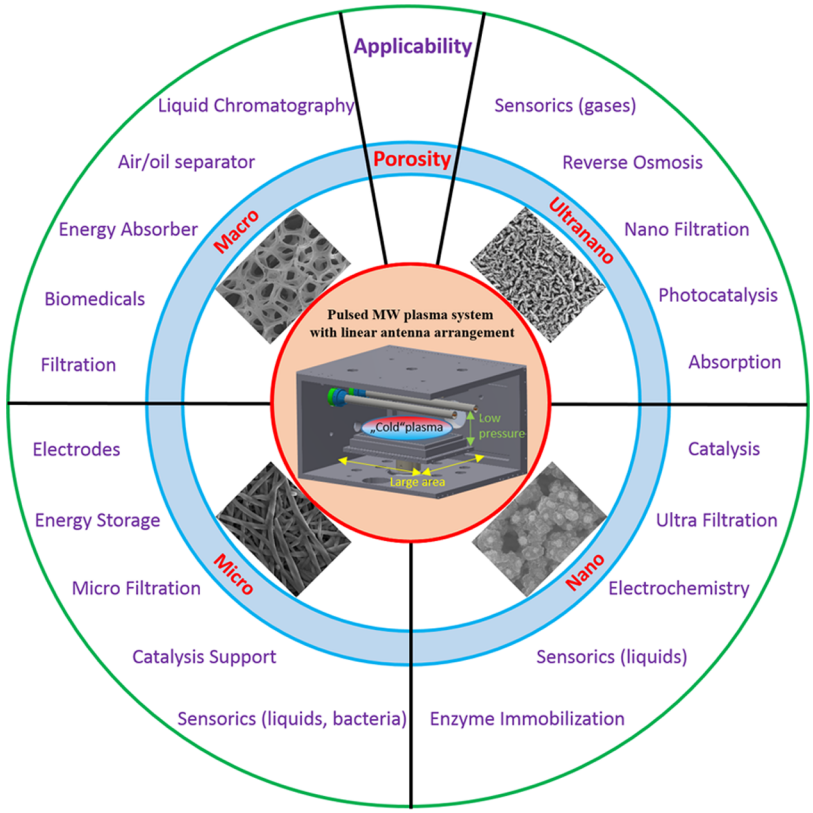

Figure 6. Classification of porous diamond structures by pore size and their potential applicability.

LAMWP system, is minimally affected by the deposition temperature. In this sense, the LAMWP system is suitable for porous diamond growth on temperature-sensitive substrates over a large area. The multilayered structures (sandwich and two-layer compartment structures) can be prepared within a single deposition run by simply varying the gas chemistry during the CVD process. This saves fabrication time. It should be noted that all of the fabricated and presented diamond-based porous structures were thick enough to be self-standing.

3.3. Applicability of Porous Diamond Structures. Generally, porous materials are of significant interest due to their wide applications. They can be used for various targets in solar energy systems containing adsorption materials, thermal energy storage materials, insulation materials, evaporation materials, or heat transfer augmentation materials.[61] The distribution of the sizes, shapes, and volumes of the void spaces in porous materials is directly related to their ability to perform the desired function in a particular application.[62] In addition, the material of the porous structure itself is a key factor for its usability. Porous diamond-based structures in various forms, as well as their applicability, have already been presented as promising electrodes,[26] as separators in biotechnology and biomedicine,[17] as electrochemical separators,[63] and as supercapacitors.[32] In a wider manner, Figure 6 summarizes the classification of porous diamond structures grown by LAMWP on the basis of their pore sizes and outlines their potential applicability.

Driven by the demand for porous structures based on intrinsic or boron-doped diamond, the last two decades have seen an enormous effort by researchers to prepare and optimize the fabrication procedures. For example, Kondo et al. reported a two-step thermal treatment method for the fabrication of porous conductive boron-doped diamond electrodes,[64] Ruffinatto et al. reported that heavily boron-doped diamond porous membranes were fabricated using low-cost commercial fiber glass filters seeded through the Buchner filtration process,[30] Shimoni et al. presented recipes for the creation of various diamond-based patterns using a lithography-based procedurs,[65] and Gao et al. reported the preparation of a porous diamond foam by a fabrication procedure consisting of several steps.[29] Generally, a complex fabrication procedure was needed.

In this sense, we believe that our summary of the fabrication (with or without a template) of a wide range of 3D porous diamond structures using the pulsed microwave cold plasma system with a linear antenna arrangement can promote the potential use of porous diamond in industrial applications.

4. CONCLUSIONS

In this work, we reviewed two different fabrication approaches (top-down and bottom-up) of porous diamond structures in one unique CVD system, the large-area pulsed microwave plasma system with a linear antenna arrangement. In the first approach, templated diamond growth on macro-, micro-, and nanoporous substrates was presented. Low-pressure operation (10 Pa) lengthened the diamond growth in the substrate *Z*-depth and thus enhanced the penetration of the growth species into the porous templates. Moreover, thanks to the larger distance between antennas and substrate, the LAMWP system also enabled quite homogeneous two-sided deposition growth in the volume of thick or very dense porous templates within a single deposition run. In the second approach, the new plasmochemically driven growth for a high CO_2 content (80% to H_2) in the gas mixture led to an unconventional formation of dendritelike diamond films. This unique bottom-up porous

DOI: 10.1021/acsomega.9b00323
ACS Omega 2019, 4, 8441−8450

diamond growth was not dependent on the substrate material, the deposition time, or the film thickness. The results presented here demonstrate that the large-area pulsed microwave plasma system with a linear antenna arrangement is a promising and industrially compatible versatile tool for the fabrication of a great variety of porous diamond structures in a broad range of temperatures.

AUTHOR INFORMATION

Corresponding Author

*E-mail: varga@fzu.cz.

ORCID

Marián Varga: 0000-0002-9613-4614

Author Contributions

M.V. and A.K. conceived and supervised the work. M.V. was primarily responsible for preparing the macro- and nanosized structures. M.D. was responsible for the microsized structures. O.B. and Š.P. were responsible for preparing the block-stone and dendritelike structures. T.I. measured the Raman spectra. All authors contributed to preparing the manuscript and have approved the final version.

Notes

The authors declare no competing financial interest.

ACKNOWLEDGMENTS

This work was supported by the Ministry of Health of the Czech Republic grant No. AZV 15-33018A (A.K., T.I.). M.V. acknowledges GACR-FWF bilateral project (16-34856L, AI0234421), and S.P. acknowledges the Operational Programme Research, Development and Education, financed by European Structural and Investment Funds and the Czech Ministry of Education, Youth and Sports (Project No. SOLID21—CZ.02.1.01/0.0/0.0/16_019/0000760). The authors would like to thank K. Hruska, R. Jackivova, and M. Kotlar for the SEM measurements. The authors would like to thank the JEOL European training center (Paris, France) for the cross-sectional SEM measurements of the MCD/dendrite-like diamond structure. Robin Healey (Czech Technical University in Prague) is gratefully acknowledged for his language revision of the manuscript.

REFERENCES

(1) May, P. W. Diamond thin films: a 21st-century material. *Philos. Trans. R. Soc., A* **2000**, *358*, 473−495.

(2) Gicquel, A.; Hassouni, K.; Silva, F.; Achard, J. CVD diamond films: from growth to applications. *Curr. Appl. Phys.* **2001**, *1*, 479−496.

(3) Nebel, C. E.; Rezek, B.; Shin, D.; Uetsuka, H.; Yang, N. Diamond for bio-sensor applications. *J. Phys. D: Appl. Phys.* **2007**, *40*, 6443−6466.

(4) Liu, H.; Wang, C.; Gao, C.; Han, Y.; Luo, J.; Zou, G.; Wen, C. New insights into selected-area deposition of diamond films by means of selective seeding. *J. Phys.: Condens. Matter* **2002**, *14*, 10973−10977.

(5) Huff, M. A.; Aidala, D. A.; Butler, J. E. MEMS applications using diamond thin films. *Solid State Technol.* **2006**, *49*, 45−46.

(6) Kromka, A.; Babchenko, O.; Rezek, B.; Ledinsky, M.; Hruska, K.; Potmesil, J.; Vanecek, M. Simplified procedure for patterned growth of nanocrystalline diamond micro-structures. *Thin Solid Films* **2009**, *518*, 343−347.

(7) Gavrilov, S. A.; Dzbanovsky, N. N.; Il'ichev, É. A.; Minakov, P. V.; Poltoratsky, É. A.; Rychkov, G. S.; Suetin, N. V. Electron flow enhancement with a diamond membrane. *Tech. Phys.* **2004**, *49*, 108−113.

(8) Davydova, M.; Kromka, A.; Rezek, B.; Babchenko, O.; Stuchlik, M.; Hruska, K. Fabrication of diamond nanorods for gas sensing applications. *Appl. Surf. Sci.* **2010**, *256*, 5602−5605.

(9) Yang, N.; Uetsuka, H.; Osawa, E.; Nebel, C. E. Vertically Aligned Diamond Nanowires for DNA Sensing. *Angew. Chem., Int. Ed.* **2008**, *47*, 5183−5185.

(10) Kondo, T.; Lee, S.; Honda, K.; Kawai, T. Conductive diamond hollow fiber membranes. *Electrochem. Commun.* **2009**, *11*, 1688−1691.

(11) Mehedi, H.; Arnault, J.-C.; Eon, D.; Hébert, C.; Carole, D.; Omnes, F.; Gheeraert, E. Etching mechanism of diamond by Ni nanoparticles for fabrication of nanopores. *Carbon* **2013**, *59*, 448−456.

(12) Matsumoto, H.; Tanioka, A. Functionality in Electrospun Nanofibrous Membranes Based on Fiber's Size, Surface Area, and Molecular Orientation. *Membranes* **2011**, *1*, 249−264.

(13) Hébert, C.; Scorsone, E.; Bendali, A.; Kiran, R.; Cottance, M.; Girard, H. A.; Degardin, J.; Dubus, E.; Lissorgues, G.; Rousseau, L.; Mailley, P.; Picaud, S.; Bergonzo, P. Boron doped diamond biotechnology: from sensors to neurointerfaces. *Faraday Discuss.* **2014**, *172*, 47−59.

(14) Siuzdak, K.; Bogdanowicz, R. Nano-engineered Diamond-based Materials for Supercapacitor Electrodes: A Review. *Energy Technol.* **2018**, *6*, 223−237.

(15) Yang, N.; Foord, J. S.; Jiang, X. Diamond electrochemistry at the nanoscale: A review. *Carbon* **2016**, *99*, 90−110.

(16) Kriele, A.; Williams, O. A.; Wolfer, M.; Hees, J. J.; Smirnov, W.; Nebel, C. E. Formation of nano-pores in nano-crystalline diamond films. *Chem. Phys. Lett.* **2011**, *507*, 253−259.

(17) Aramesh, M.; Fox, K.; Lau, D. W. M.; Fang, J.; Ken Ostrikov, K.; Prawer, S.; Cervenka, J. Multifunctional three-dimensional nanodiamond-nanoporous alumina nanoarchitectures. *Carbon* **2014**, *75*, 452−464.

(18) Smirnov, W.; Hees, J. J.; Brink, D.; Müller-Sebert, W.; Kriele, A.; Williams, O. A.; Nebel, C. E. Anisotropic etching of diamond by molten Ni particles. *Appl. Phys. Lett.* **2010**, *97*, No. 073117.

(19) Potocký, Š.; Ižák, T.; Rezek, B.; Tesárek, P.; Kromka, A. Transformation of polymer composite nanofibers to diamond fibers and films by microwave plasma-enhanced CVD process. *Appl. Surf. Sci.* **2014**, *312*, 188−191.

(20) Scorsone, E.; Saada, S.; Arnault, J. C.; Bergonzo, P. Enhanced control of diamond nanoparticle seeding using a polymer matrix. *J. Appl. Phys.* **2009**, *106*, No. 014908.

(21) Hébert, C.; Scorsone, E.; Mermoux, M.; Bergonzo, P. Porous diamond with high electrochemical performance. *Carbon* **2015**, *90*, 102−109.

(22) Suo, N.; Huang, H.; Wu, A.; Cao, G.; Hou, X.; Zhang, G. Porous boron doped diamonds as metal-free catalysts for the oxygen reduction reaction in alkaline solution. *Appl. Surf. Sci.* **2018**, *439*, 329−335.

(23) Yang, K.-H.; Nguyen, A. K.; Goering, P. L.; Sumant, A. V.; Narayan, R. J. Ultrananocrystalline diamond-coated nanoporous membranes support SK-N-SH neuroblastoma endothelial cell attachment. *Interface Focus* **2018**, *8*, No. 20170063.

(24) Varga, M.; Vretenar, V.; Izak, T.; Skakalova, V.; Kromka, A. Carbon nanotubes overgrown and ingrown with nanocrystalline diamond deposited by different CVD plasma systems. *Phys. Status Solidi B* **2014**, *251*, 2413−2419.

(25) Marton, M.; Vojs, M.; Kotlár, M.; Michniak, P.; Vančo, L'.; Veselý, M.; Redhammer, R. Deposition of boron doped diamond and carbon nanomaterials on graphite foam electrodes. *Appl. Surf. Sci.* **2014**, *312*, 139−144.

(26) Zanin, H.; May, P. W.; Fermin, D. J.; Plana, D.; Vieira, S. M. C.; Milne, W. I.; Corat, E. J. Porous Boron-Doped Diamond/Carbon Nanotube Electrodes. *ACS Appl. Mater. Interfaces* **2014**, *6*, 990−995.

(27) Varga, M.; Stehlik, S.; Kaman, O.; Izak, T.; Domonkos, M.; Lee, D. S.; Kromka, A. Templated diamond growth on porous carbon foam decorated with poly(vinyl alcohol)-nanodiamond composite. *Carbon* **2017**, *119*, 124−132.

DOI: 10.1021/acsomega.9b00323
ACS Omega 2019, 4, 8441−8450

(28) Silva, A. A.; Pinheiro, R. A.; do Amaral Razzino, C.; Trava-Airoldi, V. J.; Corat, E. J. Thin-film nanocomposites of BDD/CNT deposited on carbon fiber. *Diamond Relat. Mater.* **2017**, *75*, 116−122.
(29) Gao, F.; Wolfer, M. T.; Nebel, C. E. Highly porous diamond foam as a thin-film micro-supercapacitor material. *Carbon* **2014**, *80*, 833−840.
(30) Ruffinatto, S.; Girard, H. A.; Becher, F.; Arnault, J.-C.; Tromson, D.; Bergonzo, P. Diamond porous membranes: A material toward analytical chemistry. *Diamond Relat. Mater.* **2015**, *55*, 123−130.
(31) Petrák, V.; Vlčková Živcová, Z.; Krýsová, H.; Frank, O.; Zukal, A.; Klimša, L.; Kopeček, J.; Taylor, A.; Kavan, L.; Mortet, V. Fabrication of porous boron-doped diamond on SiO2 fiber templates. *Carbon* **2017**, *114*, 457−464.
(32) Gao, F.; Nebel, C. E. Diamond-Based Supercapacitors: Realization and Properties. *ACS Appl. Mater. Interfaces* **2015**, *8*, 28244−28254.
(33) Kromka, A.; Babchenko, O.; Kozak, H.; Hruska, K.; Rezek, B.; Ledinsky, M.; Potmesil, J.; Michalka, M.; Vanecek, M. Seeding of polymer substrates for nanocrystalline diamond film growth. *Diamond Relat. Mater.* **2009**, *18*, 734−739.
(34) Varga, M.; Potocky, S.; Tesarek, P.; Babchenko, O.; Davydova, M.; Kromka, A. Diamond growth on copper rods from polymer composite nanofibres. *Appl. Surf. Sci.* **2014**, *312*, 220−225.
(35) Kato, H.; Hees, J.; Hoffmann, R.; Wolfer, M.; Yang, N.; Yamasaki, S.; Nebel, C. E. Diamond foam electrodes for electrochemical applications. *Electrochem. Commun.* **2013**, *33*, 88−91.
(36) Alexeev, A. M.; Ismagilov, R. R.; Ashkinazi, E. E.; Orekhov, A. S.; Malykhin, S. A.; Obraztsov, A. N. Diamond platelets produced by chemical vapor deposition. *Diamond Relat. Mater.* **2016**, *65*, 13−16.
(37) Drijkoningen, S.; Pobedinskas, P.; Korneychuk, S.; Momot, A.; Balasubramaniam, Y.; Van Bael, M. K.; Turner, S.; Verbeeck, J.; Nesládek, M.; Haenen, K. On the Origin of Diamond Plates Deposited at Low Temperature. *Cryst. Growth Des.* **2017**, *17*, 4306−4314.
(38) Schlemm, H.; Fritzsche, M.; Roth, D. Linear radio frequency plasma sources for large scale industrial applications in photovoltaics. *Surf. Coat. Technol.* **2005**, *200*, 958−961.
(39) Kromka, A.; Babchenko, O.; Izak, T.; Hruska, K.; Rezek, B. Linear antenna microwave plasma CVD deposition of diamond films over large areas. *Vacuum* **2012**, *86*, 776−779.
(40) Obrusník, A.; Bonaventura, Z. Studying a low-pressure microwave coaxial discharge in hydrogen using a mixed 2D/3D fluid model. *J. Phys. D: Appl. Phys.* **2015**, *48*, No. 065201.
(41) Tsugawa, K.; Ishihara, M.; Kim, J.; Hasegawa, M.; Koga, Y. Large-Area and Low-Temperature Nanodiamond Coating by Microwave Plasma Chemical Vapor Deposition. *New Diamond Front. Carbon Technol.* **2006**, *16*, 337−346.
(42) Izak, T.; Babchenko, O.; Varga, M.; Potocky, S.; Kromka, A. Low temperature diamond growth by linear antenna plasma CVD over large area. *Phys. Status Solidi B* **2012**, *249*, 2600−2603.
(43) Babchenko, O.; Potocký, Š.; Ižák, T.; Hruška, K.; Bryknar, Z.; Kromka, A. Influence of surface wave plasma deposition conditions on diamond growth regime. *Surf. Coat. Technol.* **2015**, *271*, 74−79.
(44) www.ergaerospace.com.
(45) Varga, M.; Vretenar, V.; Kotlar, M.; Skakalova, V.; Kromka, A. Fabrication of free-standing pure carbon-based composite material with the combination of sp2−sp3 hybridizations. *Appl. Surf. Sci.* **2014**, *308*, 211−215.
(46) Kromka, A.; Jira, J.; Stenclova, P.; Kriha, V.; Kozak, H.; Beranova, J.; Vretenar, V.; Skakalova, V.; Rezek, B. Bacterial response to nanodiamonds and graphene oxide sheets: Bacterial response to nanodiamonds and graphene oxide. *Phys. Status Solidi B* **2016**, *253*, 2481−2485.
(47) Filik, J. Raman spectroscopy: a simple, non-destructive way to characterise diamond and diamond-like materials. *Spectrosc. Eur.* **2005**, *17*, 10−17.
(48) Kromka, A.; Babchenko, O.; Izak, T.; Varga, M.; Davydova, M.; Kratka, M.; Rezek, B. Diamond Films Deposited by Oxygen-Enhanced Linear Plasma Chemistry. *Adv. Sci. Eng. Med.* **2013**, *5*, 509−514.
(49) Joshi, A.; Nimmagadda, R. Erosion of diamond films and graphite in oxygen plasma. *J. Mater. Res.* **1991**, *6*, 1484−1490.
(50) Angus, J. C.; Sunkara, M. K.; et al. Twinning and faceting in early stages of diamond growth by chemical vapor deposition. *J. Mater. Res.* **1992**, *7*, 3001−3009.
(51) Chen, H.-G.; Chang, L.; Cho, S.-Y.; Yan, J.-K.; Lu, C.-A. Growth of Diamond Nanoplatelets by CVD. *Chem. Vap. Deposition* **2008**, *14*, 247−255.
(52) Chen, H.-G.; Chang, L. Characterization of diamond nanoplatelets. *Diamond Relat. Mater.* **2004**, *13*, 590−594.
(53) Lu, C.-A.; Chang, L. Microstructural investigation of hexagonal-shaped diamond nanoplatelets grown by microwave plasma chemical vapor deposition. *Mater. Chem. Phys.* **2005**, *92*, 48−53.
(54) Bachmann, P. K.; Leers, D.; Lydtin, H. Towards a general concept of diamond chemical vapour deposition. *Diamond Relat. Mater.* **1991**, *1*, 1−12.
(55) Potocký, Š.; Babchenko, O.; Hruška, K.; Kromka, A. Linear antenna microwave plasma CVD diamond deposition at the edge of no-growth region of C-H-O ternary diagram. *Phys. Status Solidi B* **2012**, *249*, 2612−2615.
(56) Eaton, S. C.; Sunkara, M. K. Construction of a new C−H−O ternary diagram for diamond deposition from the vapor phase. *Diamond Relat. Mater.* **2000**, *9*, 1320−1326.
(57) Wei, J.; Kawarada, H.; Suzuki, J.; Hiraki, A. Growth of diamond films at low pressure using magneto-microwave plasma CVD. *J. Cryst. Growth* **1990**, *99*, 1201−1205.
(58) Stehlik, S.; Varga, M.; Ledinsky, M.; Miliaieva, D.; Kozak, H.; Skakalova, V.; Mangler, C.; Pennycook, T. J.; Meyer, J. C.; Kromka, A.; Rezek, B. High-yield fabrication and properties of 1.4 nm nanodiamonds with narrow size distribution. *Sci. Rep.* **2016**, *6*, No. 38419.
(59) Barnard, A. S.; Russo, S. P.; Snook, I. K. Surface structure of cubic diamond nanowires. *Surf. Sci.* **2003**, *538*, 204−210.
(60) Barnard, A. S. Structural properties of diamond nanowires: Theoretical predictions and experimental progress. *Rev. Adv. Mater. Sci.* **2004**, *6*, 94−119.
(61) Rashidi, S.; Esfahani, J. A.; Rashidi, A. A review on the applications of porous materials in solar energy systems. *Renewable Sustainable Energy Rev.* **2017**, *73*, 1198−1210.
(62) Davis, M. E. Ordered porous materials for emerging applications. *Nature* **2002**, *417*, 813−821.
(63) Gao, F.; Nebel, C. E. Electrically Conductive Diamond Membrane for Electrochemical Separation Processes. *ACS Appl. Mater. Interfaces* **2016**, *8*, 18640−18646.
(64) Kondo, T.; Kodama, Y.; Ikezoe, S.; Yajima, K.; Aikawa, T.; Yuasa, M. Porous boron-doped diamond electrodes fabricated via two-step thermal treatment. *Carbon* **2014**, *77*, 783−789.
(65) Shimoni, O.; Cervenka, J.; Karle, T. J.; Fox, K.; Gibson, B. C.; Tomljenovic-Hanic, S.; Greentree, A. D.; Prawer, S. Development of a Templated Approach to Fabricate Diamond Patterns on Various Substrates. *ACS Appl. Mater. Interfaces* **2014**, *6*, 8894−8902.

DOI: 10.1021/acsomega.9b00323
ACS Omega 2019, 4, 8441−8450